UNSTEADY MHD FLOW OF AN EYRING-POWELL NANOFLUID OF NTH-ORDER CHEMICAL REACTION NEAR STAGNATION POINT PAST A CONVECTIVELY HEATED STRETCHING SHEET IN THE PRESENCE OF THERMAL RADIATION AND INTERNAL HEAT GENERATION IN A POROUS MEDIUM

Supported by tetfund

P. O. Olanrewaju[1]*, A. M. Olanrewaju[2], R. A. Adelagun[3] and F. E. James[1]
[1]Department of Mathematics and Statistics, Federal University Wukari, Taraba State, Nigeria
[2]Department of Mathematics, Covenant University, Ota, Ogun State, Nigeria
[3]Department of Chemical Sciences, Federal University Wukari, Taraba State, Nigeria
*Corresponding author: oladapo_anu@yahoo.ie

Received: September 10, 2020 **Accepted:** November 19, 2020

Abstract: The objective of this article is to scrutinize the unsteady MHD flow near a stagnation of chemically reacting Powell-Eyring nanofluid over a convectively heated stretched surface using the impact of thermal radiation, internal heat generation, thermal and solutal buoyancy with magnetic field intensity. The highly non-linear partial differential equations are transformed into ordinary differential equations by similarity transformation and later handles by shooting procedure alongside with sixth-order Runge Kutta iterative scheme. Comparative reviews between the published articles were made with the present study and excellent agreements were established. Effectiveness of innumerable fluid flow embedded parameters is publicized graphically on velocity, temperature and concentration graphs. It is manifested that fluid velocity promotes with the larger values of fluid parameter, unsteady parameter, stretching parameter, radiation parameter, and internal heat generation parameter. It is also observed that concentration declines when destructive chemical reaction, solutal buoyancy, and stretching parameter enhances whilst the antithesis direction is noticed in the order of chemical reaction parameter. Furthermore, the thermal boundary layer thickness thickens with enhancing unsteady parameter. We further examined the influence of this fluid flow parameters on the skin friction coefficient, Nusselt number and Sherwood number.

Keywords: Buoyancy forces, Powell-Eyring nanofluid, unsteady MHD flow, stagnation point

Introduction

Magnetohydrodynamics (MHD) is an aspect of science that deals with the mutual interaction between the magnetic fields and moving electrically conducting fluid. Hydromagnetic phenomenon plays a vital role reason been that it has prevalent use in industries and engineering, like automotive fuel level indicator, accelerators, nuclear reactors, electroslag remelting, refinement of alloys, magnetometers, electronic motors, transformers and so on. Alfvé, (1942) was the first to initiate the area of hydromagnetic and many other researchers like Bhatti *et al*. (2016), Srinivas *et al*. (2014), Reddy (2016), Ghadikolaeia *et al*. (2017) further discussed MHD on the flow of various geometries.

Nanofluid, which was first discovered by the Argonne laboratory, is a nanotechnology-based heat transfer fluid. This fluid consists of particles which are suspended inside conventional heat transfer liquid or base fluid. The reason of this suspension is to escalate thermal conductivity and convective heat transfer performance of this base fluid. These nanoparticles are both physical and chemical classes and are also produced by either the physical or chemical process. Nanofluids have the potential to reduce thermal resistances, and industrial groups such as electronics, medical, food and manufacturing would benefit from such improved heat transfer.

Similarly, in many industrial applications, the convectional heat transfer fluids are refrigerants, water, engine oil, ethylene glycol etc. even though an improvement in energy efficiency is possible from the topological and configuration points of view, much more is needed from the perspective of the heat transfer fluids. Despite considerable research and developmental efforts on enhanced heat transfer surfaces, major improvements in cooling capabilities have been constrained because of the poor thermal conductivities of traditional heat transfer fluids used in today's thermal management systems. In the development of any energy-efficient heat transfer fluids, the thermal conductivity enhancement in heat transfer plays a vital role. One such latest advancement in heat transfer fluids is the use of nano-sized (1–100 nm) solid particles as an additive suspended in the base fluid which is a technique for heat transfer enhancement. Improving the thermal conductivity is the key idea in enhancing the heat transfer characteristics of conventional fluids and in turn the heat transfer coefficient. Application of Nanofluids to address these issues has been the main subject of interest for many researchers around the world (Lee *et al.*, 2013; Hajjar *et al.*, 2014; Sharifpur *et al.*, 2015; Sharma *et al.*, 2016). Buongiorno (2006) discovered that the Brownian motion and thermophoresis diffusion of nanoparticles produce massive enhancement in the thermal conductivity of the fluid. Makinde and Aziz (2011) investigated the effect of Newtonian heating on flow comprising a nanoliquid towards a stretched sheet. Mohamed *et al*. (2020) explored the influence of viscous dissipation on mixed convection boundary layer flow past a vertical moving plate in a nanofluid. It was noted that there exist dual solutions in opposing flow for moving parameter range $0.18<\varepsilon<0.48$.

The efficacy of thermal radiation and internal heat generation on boundary layer flow has acquired considerable importance and it has vast applications like atomic power plant, glass production, furnace design, space vehicles, space technology streamlined rockets, satellite and many others. Olanrewaju *et al*. (2012) explored boundary layer flow of Nanofluids over a moving surface in a flowing fluid in the presence of thermal radiation and it was noted that it has a greater influence on the thermal boundary layer thickness across the flow channel. Pop *et al*. (2004) examined the characteristic of radiation impact on stagnancy point flow along an extending sheet. Makinde and Olanrewaju (2012) examined the combined effects of internal heat generation and buoyancy force on boundary layer flow over a vertical plate with a Newtonian heating. The impacts of internal heat generation and MHD pseudo-plastic nanofluid unsteady flow in a finite thin film was examined by Lin *et al*. (2015).

Recently, Ali and Zaib (2019) examined the unsteady flow of an Eyring-Powell nanofluid near stagnation point past a convectively heated stretching sheet. Furthermore, Idowu and Falohun (2020) analysed the effects of thermophoresis, Soret-

Dufour on heat and mass transfer flow of Magnetohydrodynamics non-Newtonian nanofluid over an inclined plate. Reddy *et al*. (2020) explored the activation energy impact on chemically reacting Eyring-Powell nanofluid flow over a stretching cylinder. It was recorded that the concentration declines when destructive chemical reaction enhances.

The above mentioned literature reviews confirmed that no endeavour has been made yet to examine the unsteady MHD flow of Eyring-Powell nanofluid within a stagnation point past a convectively heated stretched sheet with nth order chemical reaction, thermal radiation, internal heat generation and the magnetic field in a porous medium. With this point of view, the present study aims to fill this gap within the existing literature. The resulted nonlinear partial differential equations from the fluid flow model will be handled numerically by using shooting technique to converted nonlinear coupled partial differential equations to an initial value problems which can be handled by sixth-order Runge-Kutta iterative scheme. Graphical results are revealed for various numerous numerical values of stimulating parameters.

Flow analysis for Eyring-Powell model

We consider an unsteady flow of an incompressible viscous Eyring-Powell model from a convectively heated stretched sheet involving nanofluid. The surface is stretched in two lateral x-direction and y-direction with the velocities, respectively, in the form of $u_w(x,t)=\frac{ax}{1-ct}, u_e(x,t)=\frac{bx}{1-ct}$,

where a, b and c are constants. The basic equation of this model is described by Hayat *et al.* (2014):

$$\rho_{ij}=\mu\frac{\partial\omega_i}{\partial x_j}+\frac{1}{\sigma_1}\sinh^{-1}\left(\frac{\partial\omega_i}{E\partial x_j}\right), \quad (1)$$

Where μ is the dynamic viscosity of base fluid

$$\sinh^{-1}\left(\frac{\partial\omega_i}{E\partial x_j}\right)\cong\frac{\partial\omega_i}{E\partial x_j}-\frac{1}{6}\left(\frac{\partial\omega_i}{E\partial x_j}\right)^3, \left|\frac{\partial\omega_i}{E\partial x_j}\right|\prec\prec 1. \quad (2)$$

σ_1 and E are Eyring-Powell and rheological fluid parameters.

Flow formulation is developed by considering the impact of thermal radiation, nth order chemical reaction, and internal heat generation with buoyancy forces. A constant magnetic field of strength $B_o$is utilized in normal to y- direction. According to these assumption, the boundary layer approximation for Eyring-Powell, the governing equations can be formed as Ali and Zaib (2019):

$$\frac{\partial u}{\partial x}+\frac{\partial v}{\partial y}=0 \quad (3)$$

$$\frac{\partial u}{\partial t}+u\frac{\partial u}{\partial x}+v\frac{\partial u}{\partial y}=\left(\upsilon+\frac{1}{\rho_{nf}\sigma_{nf}E}\right)\frac{\partial^2 u}{\partial y^2}-\frac{1}{2\rho_{nf}\sigma_{nf}E^3}\left(\frac{\partial u}{\partial y}\right)^2\frac{\partial^2 u}{\partial y^2}+g\beta_T(T-T_\infty)$$
$$+g\beta_C(C-C_\infty)+\frac{\partial u_e}{\partial t}+U_e\frac{\partial u_e}{\partial x}-\frac{\sigma B_o^2}{\rho}u-\frac{\upsilon}{K}u \quad (4)$$

$$\frac{\partial T}{\partial t}+u\frac{\partial T}{\partial x}+v\frac{\partial T}{\partial y}=\alpha_{nf}\frac{\partial^2 T}{\partial y^2}+\tau\left[D_B\frac{\partial C}{\partial y}\frac{\partial T}{\partial y}+\frac{D_T}{T_\infty}\left(\frac{\partial T}{\partial y}\right)^2\right]-\frac{1}{(\rho c_p)_f}\frac{\partial q_r}{\partial y}+\frac{Q}{\rho c_p}(T-T_\infty) \quad (5)$$

$$\frac{\partial C}{\partial t}+u\frac{\partial C}{\partial x}+v\frac{\partial C}{\partial y}=D_B\frac{\partial^2 C}{\partial y^2}+\frac{D_T}{T_\infty}\left(\frac{\partial^2 T}{\partial y^2}\right)-R(C-C_\infty)^n \quad (6)$$

Subject to the following boundary conditions

$$u=u_w(x,t),\ v=0,\ -k\frac{\partial T}{\partial y}=h(t)(T_f-T),\ C=C_w\ at\ y=0$$
$$u=u_e(x,t),\ T\to T_\infty,\ C\to C_\infty\ at\ y\to\infty \quad (7)$$

The stream function ψ is defined by $u=\frac{\partial\psi}{\partial y}$ *and* $v=-\frac{\partial\psi}{\partial x}$. In order to represent the governing equations and the boundary conditions in the dimensionless form, the following similarity variables transformation were utilized as follows:

$$\eta=y\sqrt{\frac{a}{\upsilon(1-ct)}}, u=\frac{ax}{1-ct}f'(\eta), v=-\sqrt{\frac{a\upsilon}{1-ct}}f(\eta) \quad (8)$$
$$\theta(\eta)=\frac{T-T_\infty}{T_f-T_\infty}, \phi(\eta)=\frac{C-C_\infty}{C_f-C_\infty}, h(t)=\frac{d}{\sqrt{1-ct}}.$$

The radiative heat flux q_r is described by Roseland approximation such that

$$q_r=-\frac{4\sigma_s}{3k_e}\frac{\partial T^4}{\partial y}, \quad (9)$$

where σ_s *and* k_e are the Stefan-Boltzmann constant and the mean absorption coefficient, respectively. Following Shateyi *et al*. (2010), we assume that the temperature differences within the flow are sufficiently small so that the T^4 can be expressed as a linear function after using Taylor series to expand T^4 about the free stream temperature T_∞ and neglecting higher-order terms. This result is the following approximation:

$$T^4\approx 4T_\infty^3T-3T_\infty^4. \quad (10)$$

By using (9) and (10) in (5), we obtain

$$\frac{\partial q_r}{\partial y}=-\frac{16\sigma_s}{3k_e}\frac{\partial^2 T^4}{\partial y^2}. \quad (11)$$

Applying the stream function, equation (3) is identically satisfied. Similarly, by applying the relation in equations (8) and (11) into equations (4) – (7), we obtained the following dimensionless equations of the form;

$$(1+\varepsilon 1)f''' - f'^2 + ff'' - \lambda\left(\frac{\eta}{2}f'' + f'\right) - \varepsilon 1\delta\, f''^2 f''' + Gr_T\theta + Gr_C\phi - (M+P)f' + \lambda B + B^2 = 0 \tag{12}$$

$$\left(1+\frac{4}{3}Ra\right)\theta'' + \Pr Nb\,\theta'\phi' + \Pr f\theta' + \Pr Nt\,\theta'^2 - \Pr\frac{\lambda}{2}\eta\theta' + \Pr\lambda_1\theta = 0 \tag{13}$$

$$\phi'' + Le\left(f - \frac{\lambda}{2}\eta\right)\phi' + \frac{Nt}{Nb}\theta'' - LeR_1\phi^n = 0 \tag{14}$$

With the converted boundary conditions

$$f(0)=0,\ f'(0)=1,\ \theta'(0)=-\gamma(1-\theta(0)),\ \phi(0)=1$$
$$f'(\infty)=A,\ \theta(\infty)=0,\ \phi(\infty)=0 \tag{15}$$

Where primes denote the differential with respect to η. Where ε1, λ, Gr_T, Gr_C, M, P, B, Ra, Pr, Nb, Nt, λ_1, Le, R_1, γ and n represents the Eyring-Powell fluid parameter, the unsteady parameter, thermal buoyancy, solutal buoyancy, magnetic field parameter, porosity parameter, stretching parameter, thermal radiation parameter, Prandtl number, the Brownian motion parameter, the thermophoresis parameter, internal heat generation parameter, Schmidt number, chemical reaction parameter, Biotic number and the nth order of chemical reaction which are defined as

$$\varepsilon 1=\frac{1}{\mu\sigma_{nf}E},\ \lambda=\frac{c}{a},\ \delta=\frac{a^3x^2}{2\upsilon E^2(1-ct)^2},\ Gr_T=\frac{g\beta_T(T_f-T_\infty)(1-ct)^2}{a^2x},$$
$$Gr_C=\frac{g\beta_C(C_f-C_\infty)(1-ct)^2}{a^2x},\ M=\frac{\sigma B_o^2(1-ct)}{\rho_{nf}a},\ P=\frac{\upsilon(1-ct)}{Ka},\ \Pr=\frac{\upsilon}{\alpha_{nf}},$$
$$Ra=\frac{4\sigma_s T_\infty^3}{k_e(\rho c_p)_f},\ Nb=\frac{\tau D_B(C_f-C_\infty)}{\upsilon},\ Nt=\frac{\tau D_T(T_f-T_\infty)}{T_\infty\upsilon},\ Le=\frac{\upsilon}{D_B}, \tag{16}$$
$$\lambda_1=\frac{Q(1-ct)}{(\rho c_p)_f a},\ R_1=\frac{R(1-ct)}{a(C_f-C_\infty)^{1-n}},\ B=\frac{b}{a},\ \gamma=\frac{d}{k}\sqrt{\frac{\upsilon}{a}}$$

Here, the skin friction, local Nusselt number, and local Sherwood number are simplified as

$$C_f=\frac{\tau_w}{\rho U_w^2},\quad Nu_x=\frac{xq_w}{k(T_f-T_\infty)},\ Sh_x=\frac{xJ_w}{D_B(C_f-C_\infty)} \tag{17}$$

Where

$$\tau_w=\left(\mu+\frac{1}{E\sigma_{nf}}\right)\left(\frac{\partial u}{\partial y}\right)-\frac{1}{6}\left(\frac{1}{E}\frac{\partial u}{\partial y}\right)^3,\ q_w=-k\left(1+\frac{16\sigma_s T_\infty^3}{3k_e\alpha_{nf}}\right)\left(\frac{\partial T}{\partial y}\right)_{y=0} \tag{18}$$
$$J_w=-k\left(\frac{\partial C}{\partial y}\right)_{y=0}$$

Which gives

$$C_f\,\mathrm{Re}_x^{1/2}=(1+\varepsilon 1)f''(0)-\frac{1}{3}\varepsilon 1\delta(f''(0))^3=0,$$
$$Nu_x\,\mathrm{Re}_x^{-1/2}=-\theta'(0),\ Sh_x\,\mathrm{Re}_x^{-1/2}=-\phi'(0) \tag{19}$$
$$where\ \mathrm{Re}_x=\frac{xu_w}{\upsilon}\ is\ the\ \mathrm{Re}ynolds\ number.$$

Numerical procedure

Set of equations (12)- (14) together with the boundary conditions (15) was solved numerically by using Nachtsheim-Swigert shooting iteration technique alongside with Runge-Kutta sixth-order integration scheme. Here, from the process of numerical procedure, the skin-friction coefficient, the local Nusselt number and the local Sherwood number, which are respectively proportional to $f''(0), -\theta'(0)$ and $-\phi'(0)$, are also sorted out and their computational values are presented in a tabular form. The computations have been done by a program which uses a symbolic and computational computer language MAPLE (Heck, 2003). A step size of $\Delta\eta$ = 0.001 is used to be satisfactory for a convergence criterion of 10^{-10} in nearly all cases. The value of y_∞ is found to each iteration loop by the assignment statement $\eta_\infty = \eta_\infty + \Delta\eta$. The maximum value of η_∞, to each group of

parameters, $\varepsilon 1$,δ, λ, Gr_T, Gr_C, *M, P, B, Ra, Pr, Nb, Nt,* λ_1, *Le,* R_1, γ *and n* is determined when the values of unknown boundary conditions at $\eta = 0$ do not change to successful loop with error less than 10^{-10}.

Results and Discussion

The Maple software is used to run the sixth order of Runge Kutta iterative technique in order to solve the equations (12) – (14) satisfying equation (15) numerically. Pertinent embedded fluid flow parameters namely as the ε1, δ, λ, Gr_T, Gr_C, M, P, B, Ra, Pr, Nb, Nt, λ_1, Le, R_1, γ and n which represent the Eyring-Powel fluid parameters (ε, δ), the unsteady parameter, thermal buoyancy, solutal buoyancy, magnetic field parameter, porosity parameter, stretching parameter, thermal radiation parameter, Prandtl number, the Brownian motion parameter, the thermophoresis parameter, internal heat generation parameter, Schmidt number, chemical reaction parameter, Biotic number and the nth order of chemical reaction. We assigned numerical values to the fluid flow parameters based on the existing literature for easy comparison and result validation. Tables 1 & 2 showed the comparison with the previous published articles which shows perfect agreement. In Table 3, we explore the effects of all the embedded fluid flow parameter on the skin friction coefficient, local Nusselt number and the Sherwood number. Large values of λ, δ, M, P, and R_1 enhance the skin friction coefficient, while large parameter values of $\varepsilon 1, B, \lambda_1$ *and* Ra decline the skin friction coefficient. Similarly, the local Nusselt number decreases at the wall surface when larger parameter values of $\lambda, \delta, M, P, R_1, \lambda_1$ *and* Ra were used. It was later observed that the local Nusselt number was enhanced when larger values of ε and A were used. Finally, larger values of $\varepsilon 1, B, R_1, \lambda_1$ *and* Ra enhancing the Sherwood number while large values of λ, δ, M *and* P decline the rate of mass transfer at the wall surface.

Table 1: Data analysis of $f''(0)$ for different values of the unsteadiness parameter λ with $B = \delta = \varepsilon 1 = 0$

λ	Chamkha *et al*. (2010)	Mukhopadhyay *et al*. (2013)	Madhu *et al*. (2017)	Ali & Zaib (2019)	Present result
0.8	-1.261512	-1.261479	-1.261211	-1.260691	−1.26104260943
1.2	-1.378052	-1.377850	-1.377625	-1.377710	−1.37770620795

Table 2: Parameter analysis of $-\theta'(0)$ for different value of Nb and Nt for $\lambda = B = \varepsilon 1 = Ra = \lambda_1 = Gr_T = Gr_C = M = P = 0$, Le=Pr=10, γ=0.1

	Mahanthesha *et al*. (2017)	Mahanthesha *et al*. (2017)	Makinde & Aziz (2011)	Makinde & Aziz (2011)	Khan & Pop (2010)	Khan & Pop (2010)	Ali & Zaib (2019)	Ali & Zaib (2019)	Present result	Present result
Nt	Nb=0.1	Nb=0.5	Nb=0.1	Nb=0.5	Nb=0.1	Nb=0.5	Nb=0.1	Nb=0.5	Nb=0.1	Nb=0.5
0.1	0.092906	0.092907	0.0929	0.0929	0.092906	0.038324	0.092906	0.044550	0.0929073	0.03833359
0.2	0.092731	0.092732	0.0927	0.0927	0.092731	0.032497	0.092732	0.044547	0.0927325	0.03249910
0.3	0.092545	0.092545	0.0925	0.0925	0.092545	0.026905	0.092544	0.044044	0.0925451	0.02689692
0.4	0.092343	0.092344	0.0923	0.0923	0.092343	0.022010	0.092343	0.043084	0.0923436	0.02199374
0.5	0.092126	0.092126	0.0921	0.0921	0.092126	0.018034	0.092125	0.041716	0.0921259	0.01801054

Table 3: Parameter assessment of Skin friction coefficient, local Nusselt number and Sherwood number for different values of the embedded flow parameters with fixed values of Nb = Nt = 0.5, Pr =1, Le=2, γ = 0.1, $Gr_T = Gr_C = 0.5$

$\varepsilon 1$	λ	δ	B	M	P	R_1	λ_1	Ra	$-f''(0)$	$-\theta'(0)$	$-\phi'(0)$
0.1	0.1	0.1	0.1	0.1	0.1	0.1	0.1	0.1	0.78520708711928	0.074874914295989	1.001238849882
0.3	0.1	0.1	0.1	0.1	0.1	0.1	0.1	0.1	0.73792851703297	0.075508601309168	1.009547724916
0.5	0.1	0.1	0.1	0.1	0.1	0.1	0.1	0.1	0.69883749504543	0.076033052499623	1.016743850522
0.7	0.1	0.1	0.1	0.1	0.1	0.1	0.1	0.1	0.66574919936826	0.076473177593767	1.023050421482
0.1	0.15	0.1	0.1	0.1	0.1	0.1	0.1	0.1	0.79067873431149	0.073604719402050	0.983857833706
0.1	0.2	0.1	0.1	0.1	0.1	0.1	0.1	0.1	0.79494608628965	0.072012250933830	0.966622452092
0.1	0.25	0.1	0.1	0.1	0.1	0.1	0.1	0.1	0.79740637409918	0.069926860712359	0.949939965344
0.1	0.1	0.2	0.1	0.1	0.1	0.1	0.1	0.1	0.78612113808702	0.074870319961201	1.001153653041
0.1	0.1	0.3	0.1	0.1	0.1	0.1	0.1	0.1	0.78704364815004	0.074865706973317	1.001068049266
0.1	0.1	0.1	0.15	0.1	0.1	0.1	0.1	0.1	0.76963147996995	0.075515920913336	1.006163293343
0.1	0.1	0.1	0.2	0.1	0.1	0.1	0.1	0.1	0.74951039268316	0.076141357800071	1.012140487921
0.1	0.1	0.1	0.25	0.1	0.1	0.1	0.1	0.1	0.72505133149470	0.767383494738167	1.018976039285
0.1	0.1	0.1	0.1	0.2	0.1	0.1	0.1	0.1	0.82869244005642	0.074180869609937	0.993751961644
0.1	0.1	0.1	0.1	0.3	0.1	0.1	0.1	0.1	0.87032772885876	0.073477407349535	0.986785237831
0.1	0.1	0.1	0.1	0.1	0.2	0.1	0.1	0.1	0.82869244005642	0.074180869609937	0.993751961644
0.1	0.1	0.1	0.1	0.1	0.3	0.1	0.1	0.1	0.87032772885876	0.073477407349535	0.986785237831
0.1	0.1	0.1	0.1	0.1	0.1	0.3	0.1	0.1	0.79741688947289	0.074410107131997	1.191664509232
0.1	0.1	0.1	0.1	0.1	0.1	0.5	0.1	0.1	0.80677362548572	0.074069009353158	1.355236541417
0.1	0.1	0.1	0.1	0.1	0.1	0.1	0.2	0.1	0.75372031963065	0.066229328666202	1.025786574995
0.1	0.1	0.1	0.1	0.1	0.1	0.1	0.3	0.1	0.68190864015646	0.045986856760094	1.082151713256
0.1	0.1	0.1	0.1	0.1	0.1	0.1	0.1	0.3	0.77647148301185	0.073082739398187	1.004549347128
0.1	0.1	0.1	0.1	0.1	0.1	0.1	0.1	0.5	0.76839635881093	0.071429132125428	1.007764749294
0.1	0.1	0.1	0.1	0.1	0.1	0.1	0.1	0.7	0.76106804853390	0.069933392502204	1.010739329656

The effect of Eyring-Powell parameter ε on the velocity, temperature and concentration distribution was exhibited in Figs. 1, 2 & 3. It was noticed that velocity distribution enhances with an increase in the Eyring-Powell fluid parameter in Fig. 1 while the thermal boundary layer thickness and the concentration boundary layer thickness decline far away from the wall surface in Figs. 2 and 3. In Figs. 4, 5 and 6, the influence of unsteady parameter λ was exhibited on the velocity, temperature and concentration profile and it is interesting to note that enhancing the unsteady parameter λ, the velocity, temperature and concentration boundary layer thickness thickened across the flow channel. Figs. 7, 8 and 9 represent the influence of thermal Grashof number on the velocity, temperature and concentration fields.

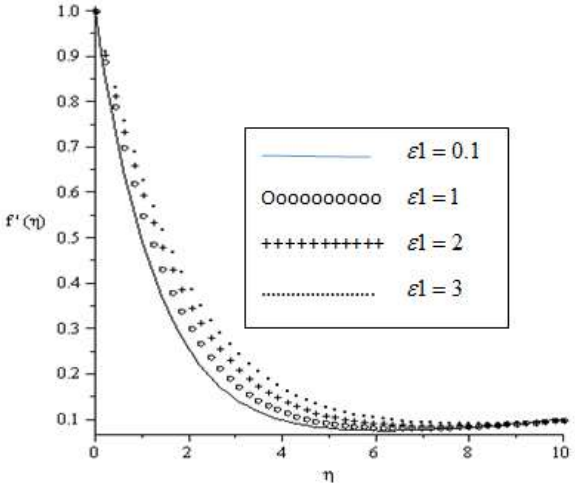

Fig. 1: Variations of ε on velocity profile when λ = δ = M= P= B= Nb= Nt= Ra= λ_1 =0.1, Pr = 1, Le =1, γ =0.2, n=1, $Gr_T = Gr_C = 0.5,\ R_1 = 0.1$

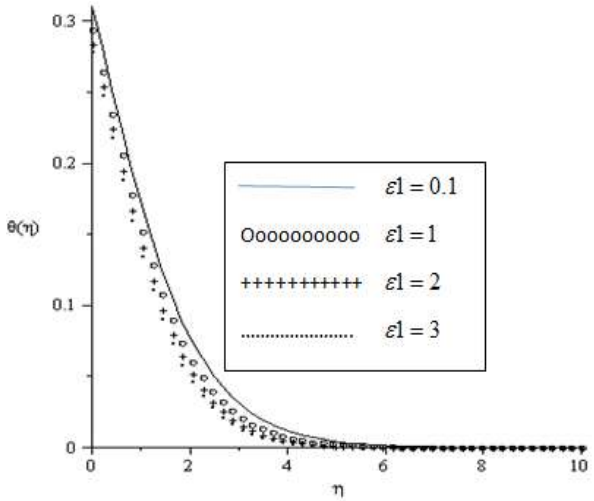

Fig. 2: Variations of ε on temperature profile when λ = δ = M= P= B= Nb= Nt= Ra= λ_1 =0.1, Pr = 1, Le =1, γ =0.2, n=1, $Gr_T = Gr_C = 0.5,\ R_1 = 0.1$

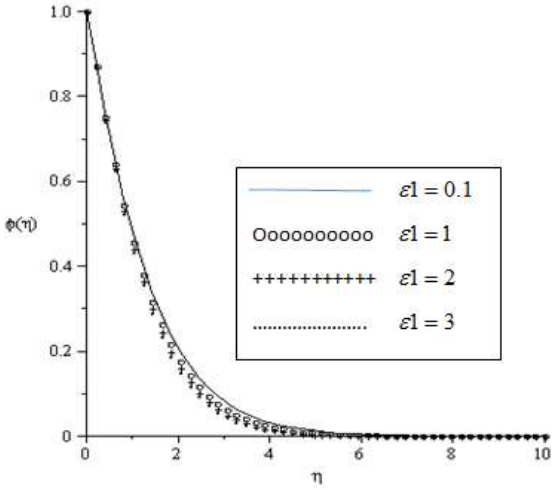

Fig. 3: Variations of ε on concentration profile when λ = δ = M= P= B= Nb= Nt= Ra= λ_1 =0.1, Pr = 1, Le =1, γ =0.2, n=1, $Gr_T = Gr_C = 0.5,\ R_1 = 0.1$

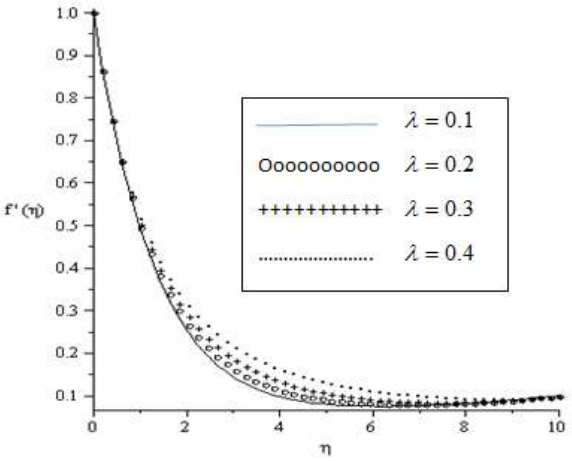

Fig. 4: Variations of λ on velocity profile when ε1 = δ = M= P= B= Nb= Nt= Ra= λ_1 =0.1, Pr = 1, Le =1, γ =0.2, n=1, $Gr_T = Gr_C = 0.5,\ R_1 = 0.1$

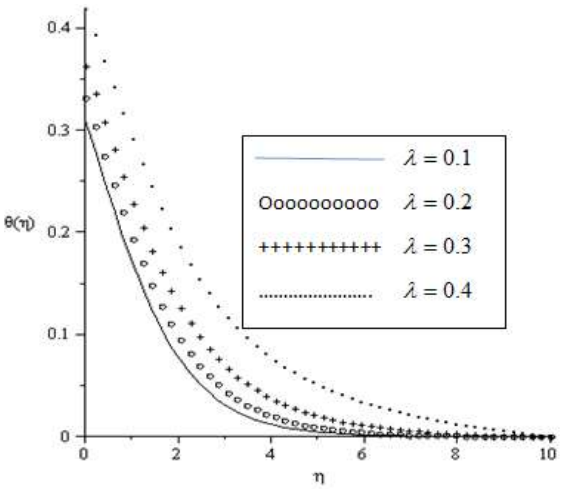

Fig. 5: Variations of λ on temperature profile when ε1 = δ = M= P= B= Nb= Nt= Ra= λ_1 =0.1, Pr = 1, Le =1, γ =0.2, n=1, $Gr_T = Gr_C = 0.5,\ R_1 = 0.1$

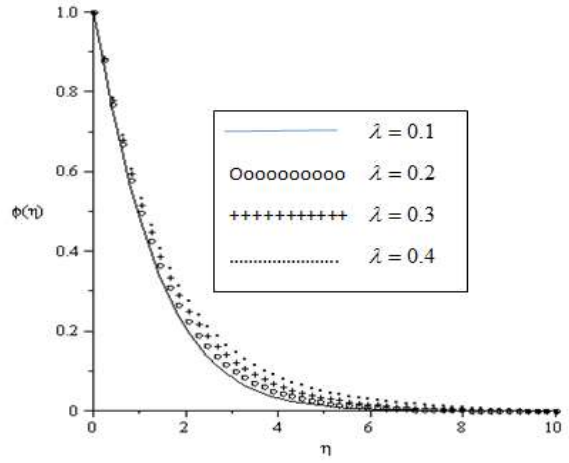

Fig. 6: Variations of λ on concentration profile when ε1 = δ = M= P= B= Nb= Nt= Ra= λ_1 =0.1, Pr = 1, Le =1, γ =0.2, n=1, $Gr_T = Gr_C = 0.5,\ R_1 = 0.1$

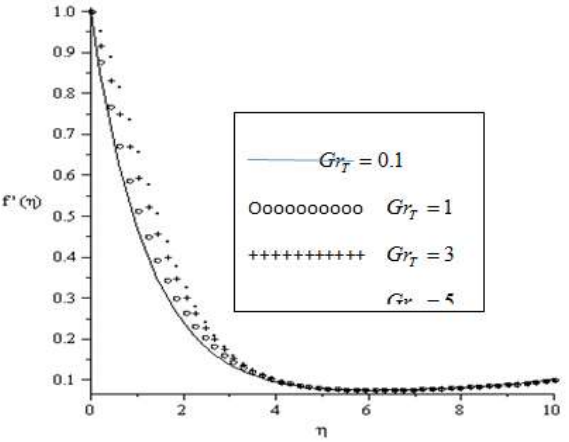

Fig. 7: Variations of Gr_T on velocity distribution when ε1 = δ = M= P= B= Nb= Nt= Ra= λ_1 =0.1, Pr = 1, Le =1, γ =0.2, n=1, $Gr_C = 0.5, \lambda = 0.1,\ R_1 = 0.1$

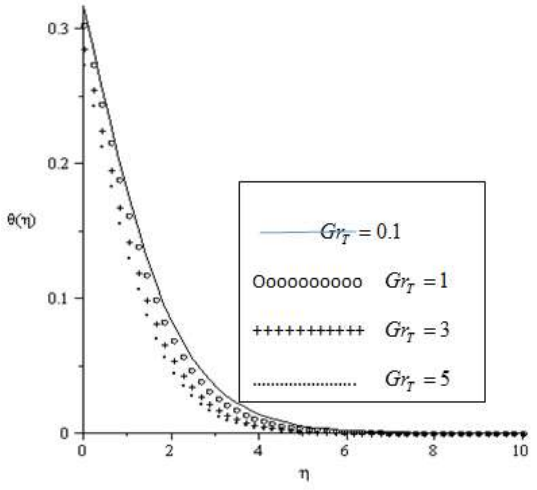

Fig. 8: Variations of Gr_T on temperature distribution when ε1 = δ = M= P= B= Nb= Nt= Ra= λ_1 =0.1, Pr = 1, Le =1, γ =0.2, n=1, $Gr_C = 0.5, \lambda = 0.1,\ R_1 = 0.1$

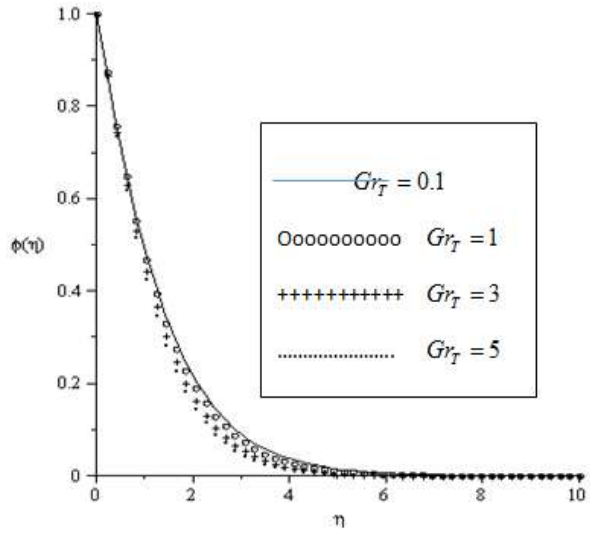

Fig. 9: Variations of Gr_T on concentration distribution when ε1 = δ = M= P= B= Nb= Nt= Ra= λ_1 =0.1, Pr = 1, Le =1, γ =0.2, n=1, $Gr_C = 0.5, \lambda = 0.1,\ R_1 = 0.1$

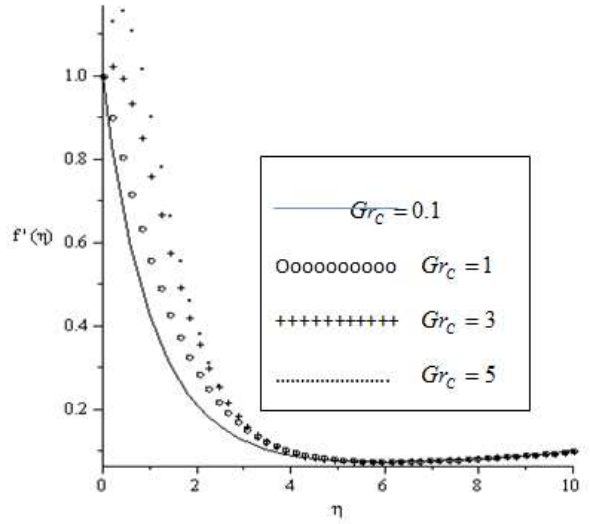

Fig. 10: Variations of Gr_C on velocity distribution when ε1 = δ = M= P= B= Nb= Nt= Ra= λ_1 =0.1, Pr = 1, Le =1, γ =0.2, n=1, $Gr_T = 0.5, \lambda = 0.1,\ R_1 = 0.1$

It was noticed that when thermal buoyancy was increased, the velocity boundary layer thickness thickened close to the wall surface in Fig. 7 while in Figs. 8 and 9, the thermal and concentration boundary layer thickness decline resulting in thinning the thermal and concentration boundary layer thickness. It can be seen also that the velocity overshoot and the buoyancy force in the buoyancy layer act as a favourable pressure gradient, which accelerates the fluid movement in the boundary layer. In Figs. 10, 11 and 12 have the same effects as Figs. 7, 8 and 9 when the solutal Grashof number was enhanced. It is worth mention that when magnetic field intensity parameter M was enhanced on the velocity profile in Fig. 13, the velocity distribution declines. From this curve, we have seen that a boost in the magnetic field parameter tends to generate the Lorentz force, which in turn cause to decline the

velocity boundary layer thickness. Enhancing the magnetic field parameter thickens the thermal and concentration boundary layer thickness in Fig. 14 and 15. The influence of porosity parameter P on the velocity, temperature and concentration profile with fixing other relevant fluid flow parameters in Fig. 16, 17 and 18 and the same effects were observed with Figs. 13, 14 and 15. Figs. 19, 20 and 21 depict the effect of stretching sheet parameter A on the velocity, temperature and concentration distribution. Enhancing parameter B enhanced the velocity boundary layer thickness and shrinks with declining values of B.

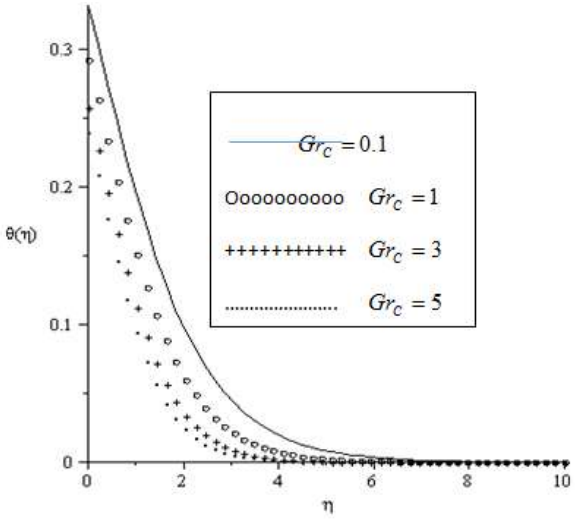

Fig. 11: Variations of Gr_C on temperature distribution when ε1 = δ = M= P= B= Nb= Nt= Ra= λ_1 =0.1, Pr = 1, Le =1, γ =0.2, n=1, $Gr_T = 0.5, \lambda = 0.1,\ R_1 = 0.1$

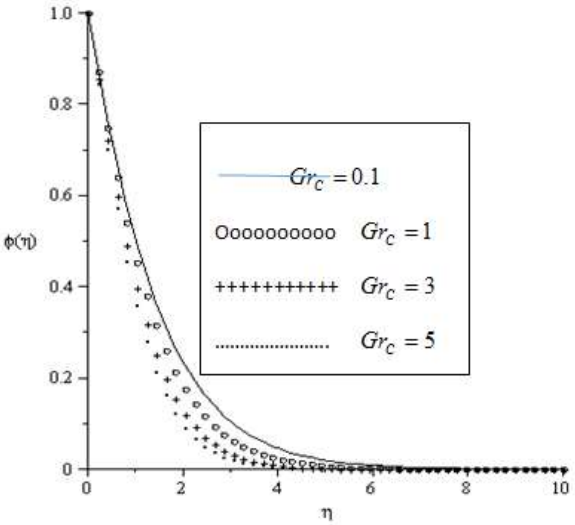

Fig. 12: Variations of Gr_C on concentration distribution when ε1 = δ = M= P= B= Nb= Nt= Ra= λ_1 =0.1, Pr = 1, Le =1, γ =0.2, n=1, $Gr_T = 0.5, \lambda = 0.1,\ R_1 = 0.1$

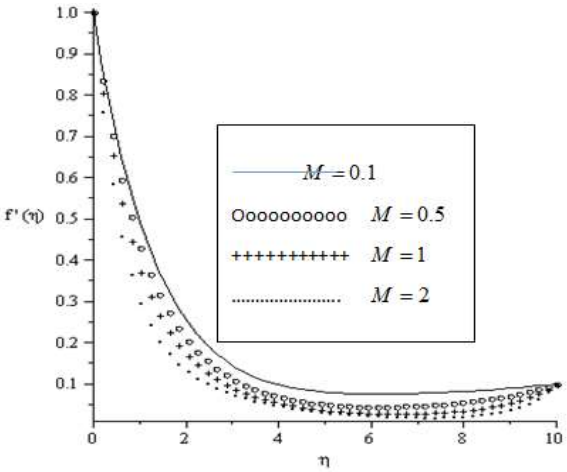

Fig. 13: Variations of M on velocity distribution when ε1 = δ = P= B= Nb= Nt= Ra= λ_1 =0.1, Pr = 1, Le =1, γ =0.2, n=1, $Gr_T = Gr_C = 0.5, \lambda = 0.1,\ R_1 = 0.1$

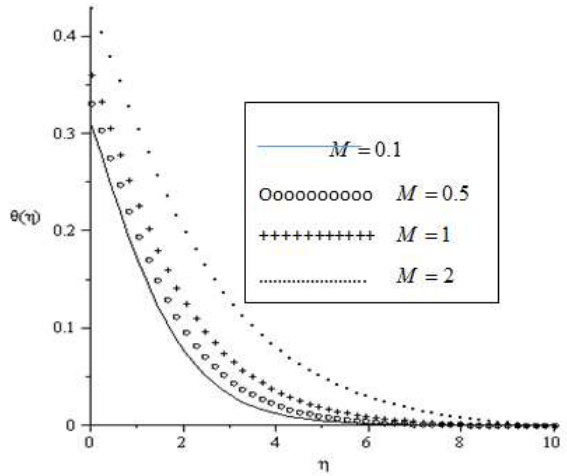

Fig. 14: Variations of M on temperature distribution when ε1 = δ = P= B= Nb= Nt= Ra= λ_1 =0.1, Pr = 1, Le =1, γ =0.2, n=1, $Gr_T = Gr_C = 0.5, \lambda = 0.1,\ R_1 = 0.1$

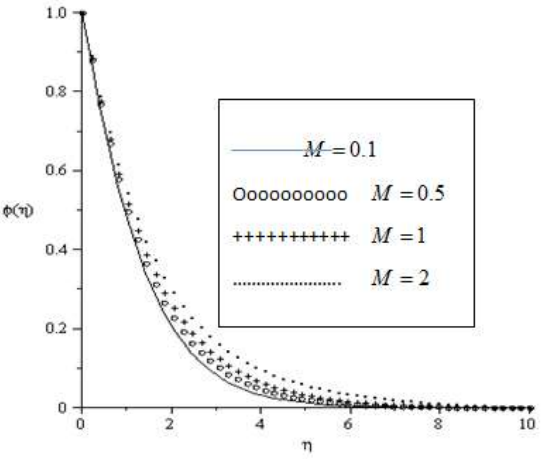

Fig. 15: Variations of M on concentration distribution when ε1 = δ = P= B= Nb= Nt= Ra= λ_1 =0.1, Pr = 1, Le =1, γ =0.2, n=1, $Gr_T = Gr_C = 0.5, \lambda = 0.1,\ R_1 = 0.1$

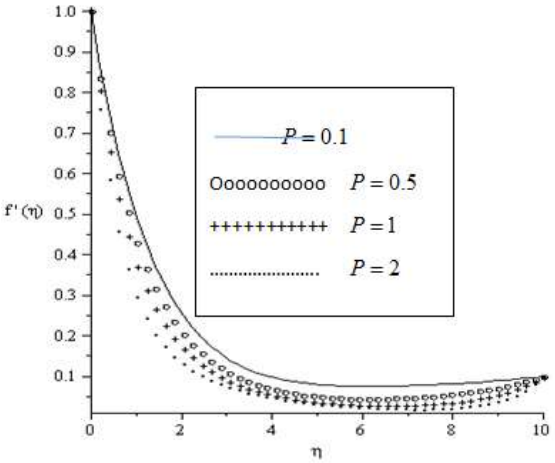

Fig. 16: Variations of P on velocity distribution when ε1 = δ = M = B= Nb= Nt= Ra= λ_1 =0.1, Pr = 1, Le =1, γ =0.2, n=1, $Gr_T = Gr_C = 0.5, \lambda = 0.1,\ R_1 = 0.1$

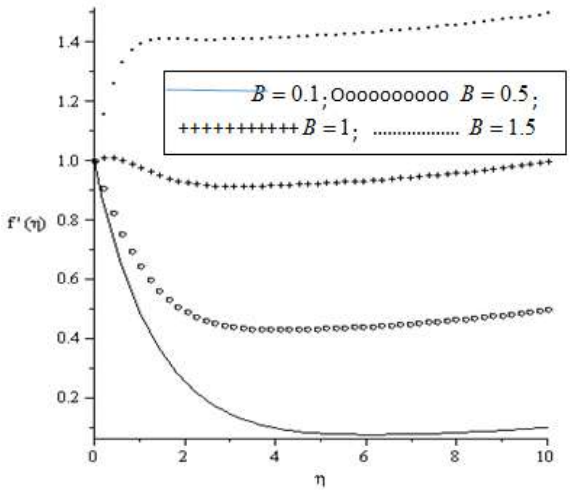

Fig. 19: Variations of A on velocity distribution when ε1 = δ = M = P= Nb= Nt= Ra= λ_1 =0.1, Pr = 1, Le =1, γ =0.2, n=1, $Gr_T = Gr_C = 0.5, \lambda = 0.1,\ R_1 = 0.1$

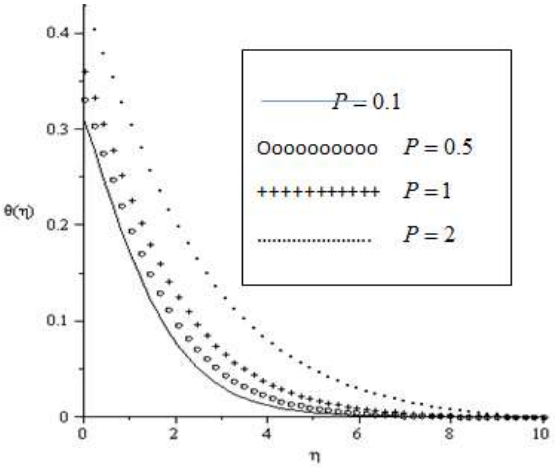

Fig. 17: Variations of P on temperature distribution when ε1 = δ = M = B= Nb= Nt= Ra= λ_1 =0.1, Pr = 1, Le =1, γ =0.2, n=1, $Gr_T = Gr_C = 0.5, \lambda = 0.1,\ R_1 = 0.1$

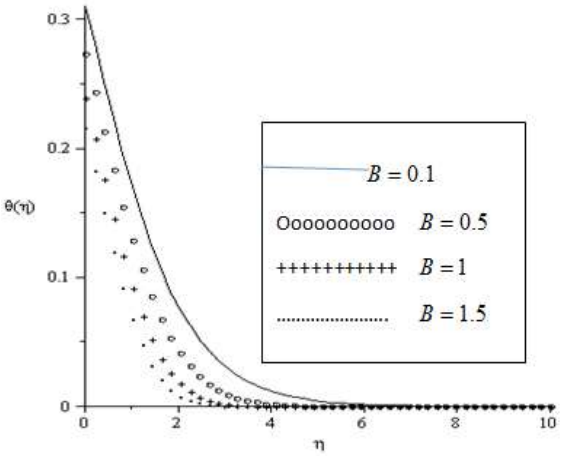

Fig. 20: Variations of A on temperature distribution when ε1 = δ = M = P= Nb= Nt= Ra= λ_1 =0.1, Pr = 1, Le =1, γ =0.2, n=1, $Gr_T = Gr_C = 0.5, \lambda = 0.1,\ R_1 = 0.1$

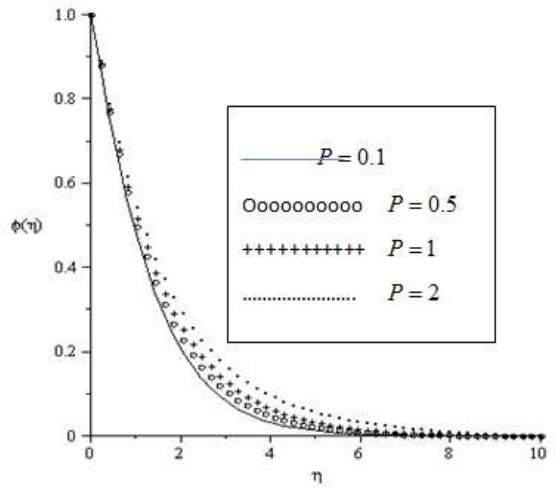

Fig. 18: Variations of P on concentration distribution when ε1 = δ = M = B= Nb= Nt= Ra= λ_1 =0.1, Pr = 1, Le =1, γ =0.2, n=1, $Gr_T = Gr_C = 0.5, \lambda = 0.1,\ R_1 = 0.1$

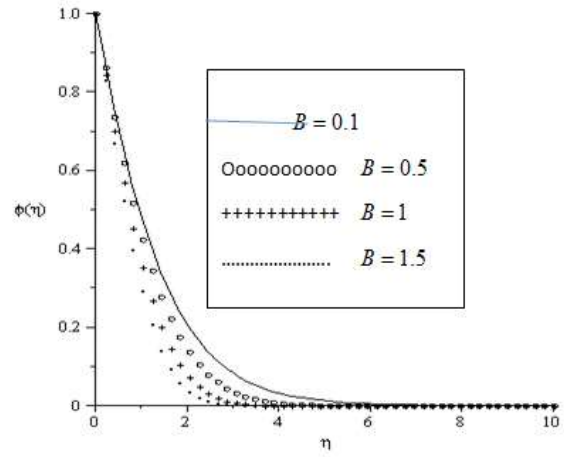

Fig. 21: Variations of A on concentration distribution when ε1 = δ = M = P= Nb= Nt= Ra= λ_1 =0.1, Pr = 1, Le =1, γ =0.2, n=1, $Gr_T = Gr_C = 0.5, \lambda = 0.1,\ R_1 = 0.1$

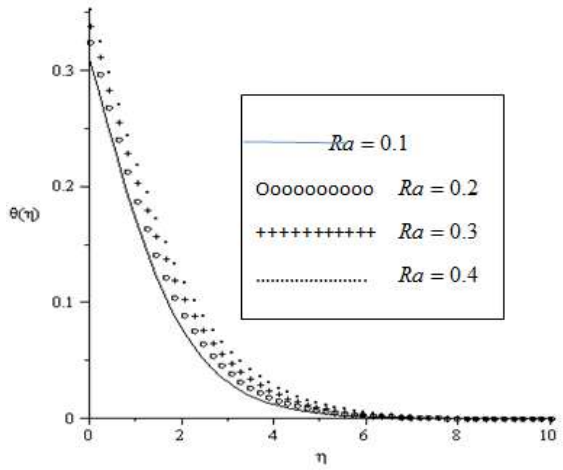

Fig. 22: Variations of Ra on temperature distribution when ε1 = δ = M = P= Nb= Nt= B = λ_1 =0.1, Pr = 1, Le =1, γ =0.2, n=1, $Gr_T = Gr_C = 0.5, \lambda = 0.1,\ R_1 = 0.1$

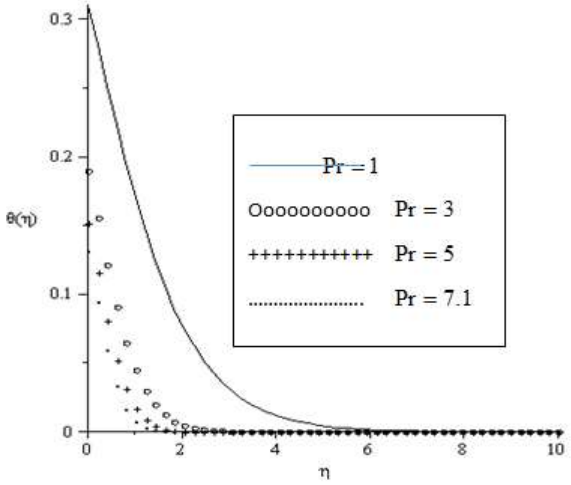

Fig. 23: Variations of Pr on temperature distribution when ε1 = δ = M = P= Nb= Nt= B = λ_1 =0.1, Ra = 0.1, Le =1, γ =0.2, n=1, $Gr_T = Gr_C = 0.5, \lambda = 0.1,\ R_1 = 0.1$

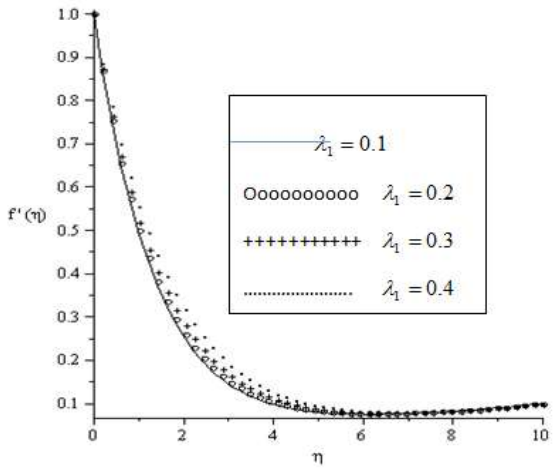

Fig. 24: Variations of λ_1 on temperature distribution when ε1 = δ = M = P= Nb= Nt= B =0.1, Pr= 1, Ra = 0.1, Le =1, γ =0.2, n=1, $Gr_T = Gr_C = 0.5, \lambda = 0.1,\ R_1 = 0.1$

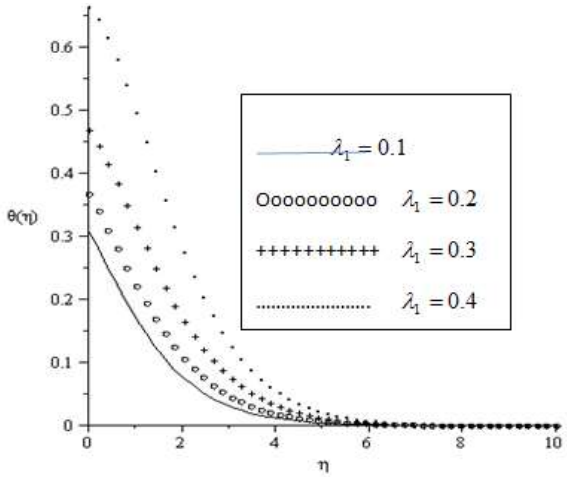

Fig. 25: Variations of λ_1 on temperature distribution when ε1 = δ = M = P= Nb= Nt= B =0.1, Pr= 1, Ra = 0.1, Le =1, γ =0.2, n=1, $Gr_T = Gr_C = 0.5, \lambda = 0.1,\ R_1 = 0.1$

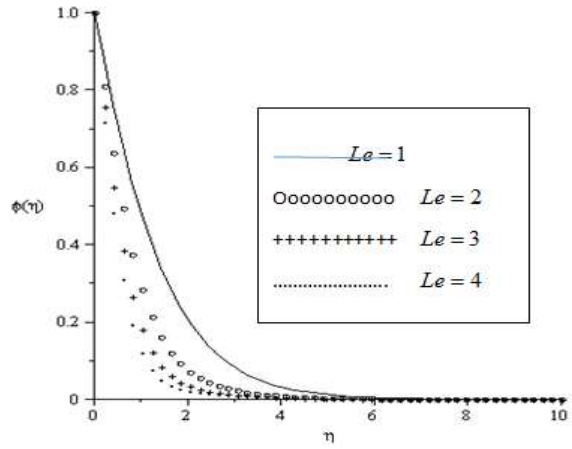

Fig. 26: Variations of Le on temperature distribution when ε1 = δ = M = P= Nb= Nt= B =0.1, Pr= 1, Ra = 0.1, λ_1 =0.1, γ =0.2, n=1, $Gr_T = Gr_C = 0.5, \lambda = 0.1,\ R_1 = 0.1$

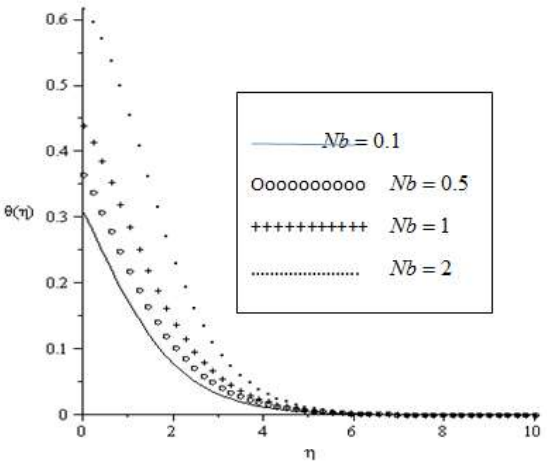

Fig. 27: Variations of Nb on temperature distribution when ε1 = δ = M = P = Nt= B =0.1, Pr= 1, Ra = 0.1, λ_1 =0.1, γ =0.2, n=1, $Gr_T = Gr_C = 0.5, \lambda = 0.1,$ Le = 1, $R_1 = 0.1$

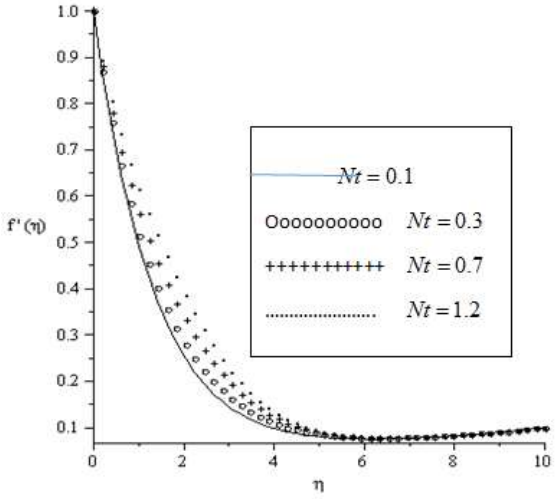

Fig. 28: Variations of Nt on velocity distribution when ε1 = δ = M = P = Nb = B =0.1, Pr= 1, Ra = 0.1, λ_1 =0.1, γ =0.2, n=1, $Gr_T = Gr_C = 0.5, \lambda = 0.1$, Le = 1, $R_1 = 0.1$

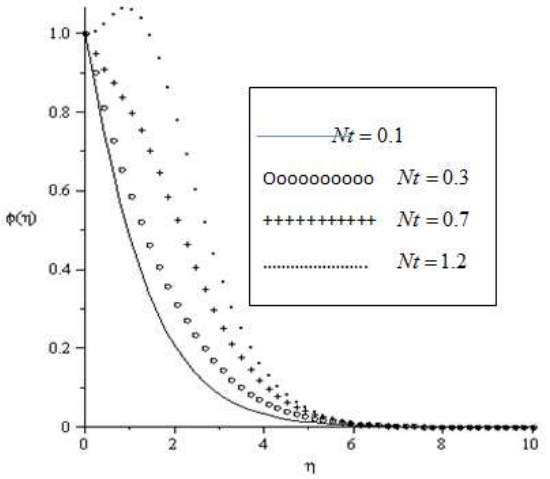

Fig. 29: Variations of Nt on concentration distribution when ε1 = δ = M = P = Nb = B =0.1, Pr= 1, Ra = 0.1, λ_1 =0.1, γ =0.2, n=1, $Gr_T = Gr_C = 0.5, \lambda = 0.1$, Le = 1, $R_1 = 0.1$

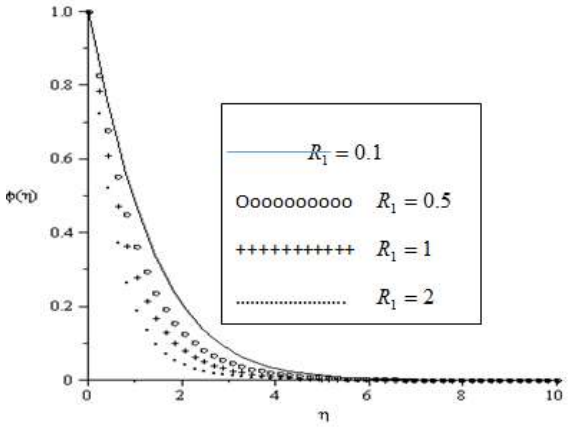

Fig. 30: Variations of R_1 on concentration distribution when ε1 = δ = M = P =Nt= Nb = B =0.1, Pr= 1, Ra = 0.1, λ_1 =0.1, γ =0.2, n=1, $Gr_T = Gr_C = 0.5, \lambda = 0.1$, Le = 1

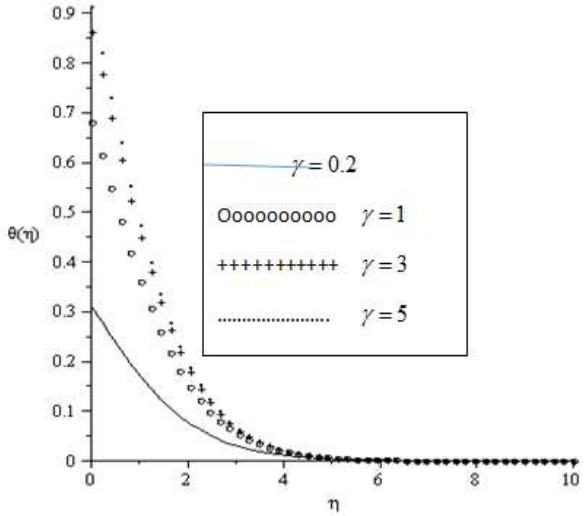

Fig. 31: Variations of γ on concentration distribution when ε1 = δ = M = P = Nt=Nb = B =0.1, Pr= 1, Ra = 0.1, λ_1 =0.1, R1=0.1, n=1, $Gr_T = Gr_C = 0.5, \lambda = 0.1$, Le = 1

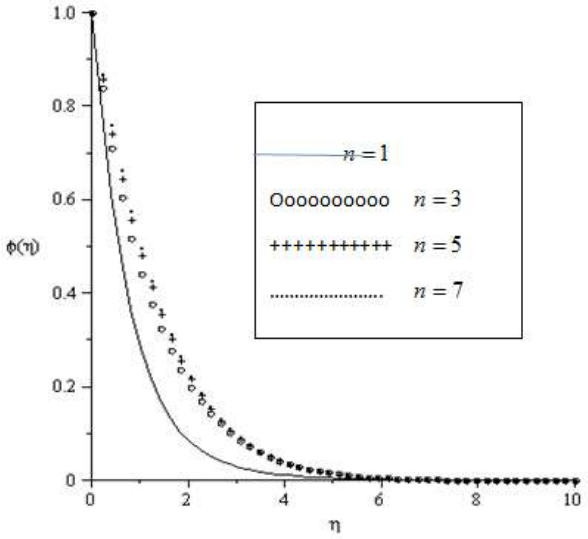

Fig. 32: Variations of n on concentration distribution when ε1 = δ = M = P = Nt=Nb = B =0.1, Pr= 1, Ra = 0.1, λ_1 =0.1, R1=0.1, γ=0.2, $Gr_T = Gr_C = 0.5, \lambda = 0.1$, Le = 1

From Figs. 20 and 21, it was seen that the thermal and concentration boundary layer thickness decrease with larger values of A. In Fig. 22, the effect of thermal radiation on thermal boundary layer thickness and it was observed that larger the thermal radiation parameter Ra, the thermal boundary layer thickness escalated. Fig. 23 depicts the graph of temperature against η for various values of Prandtl number Pr. Larger values of Pr decline the thermal boundary layer thickness across the flow channel. Figs. 24 and 25 depict the effect of internal heat generation parameter λ_1 on the velocity and temperature distribution. It is interesting to note that larger values of λ_1 enhancing the velocity and temperature profile thereby thickens the velocity and thermal boundary layer thickness across the fluid flow channel. The effect of Lewis number Le on the concentration distribution was

graphed in Fig. 26 and it was observed that larger values of Le decline the concentration distribution. The influence of Brownian motion parameter Nb was depicted in Fig. 27. The temperature of the liquid shows an increasing trend for enhancing values of Brownian motion parameter. Physically speaking, the irregular motion of fluid molecule escalates Brownian motion, thus producing the movement of nanoparticle away from the surface. Figs. 28 and 29 show that the velocity and concentration distribution climbs as the thermophoresis parameter Nt is enhanced. Effects of chemical reaction parameter R_1 on concentration curves in Fig. 30 and it is reported that the positive estimation of the chemical reaction parameter weakens the concentration distribution, thus the concentration boundary layer thickness decreases of enhancing the chemical reaction parameter. Fig. 31 depicts the effect of the Biot number γ on the temperature distribution. Enhancing the values of the convective surface boundary condition escalates the thermal boundary layer thickness across the fluid flow channel. Finally, Fig. 32 represents the influence of the order of chemical reaction n on the concentration distribution. It was observed that enhancing the order of chemical reaction thickens the concentration boundary layer thickness till certain values and has no effects on the concentration field (when steady case is reached). Here, when n= 5 & 7, there was no change in the curve.

Conclusion

Due to the importance of thermal radiation, nth order of chemical reaction, internal heat generation, we examine the MHD stagnation point Eyring-Powell nanofluid flow towards a stretching sheet with the convective surface boundary condition has been investigated. Application of shooting method was to convert the nonlinear coupled boundary value problems to an initial value problem which can now be handled by the sixth-order Runge-Kutta iterative scheme. The skin friction coefficient decline with the larger values of thermal radiation Ra, internal heat generation λ_1, stretching sheet and the Erying-Powell ε1 parameters.The skin friction coefficient enhances with rises in unsteady λ, Erying-Powell δ, magnetic field M, porosity P and chemical reaction R_1 parameters while the Sherwood and the Nusselt numbers enhanced with larger values of Eyring-Powell ε and stretching sheet B parameters. Similarly, bigger values of radiation, chemical reaction and internal heat generation escalates the Sherwood number. It was also noticed that larger values of Internal heat generation λ_1, stretching sheet B, solutal Grashof number Gr_C, thermal Grashof number Gr_T, unsteady λ and the Erying-Powell ε parameters enhances the velocity of the fluid resulting in the thickening the velocity boundary layer thickness while larger values of the buoyancies parameter are for the cooling system which was also established during the course of this research work. Bigger values of Gr_T and Gr_C decline the thermal boundary layer thickness including the concentration profile. Similarly, bigger values of Prandtl number Pr reduced the thermal boundary layer thickness while bigger values of the Lewis number Le thinning the concentration boundary layer thickness while increased values of the thermophoresis and nth order of chemical reaction parameters escalated the concentration distribution across the flow regime. Interestingly, nth order of chemical reaction will reach a stage where there is steadiness in the effect on the concentration profile. The velocity distribution diminishes when we enhance the magnetic field and porosity parameter across the fluid flow channel. It was observed that increasing the Brownian motion parameter Nb, the thermal boundary layer thickness enhances across the fluid flow regime. Finally, combined effect of the Eyring-Powell (ε1, δ) parameters, unsteady parameter, buoyancy forces parameters, magnetic field M and porosity P parameters, thermal radiation Ra parameter, Lewis number Le, Prandtl number Pr, internal heat generation λ_1, Brownian motion Nb parameter, thermophoresis Nt parameter, chemical reaction R1 parameters, Biot number γ parameter and the nth order of chemical reaction n parameter has greater influence on the MHD nanofluid flow.

Acknowledgements

The authors want to appreciate the financial assistance of TETFund (year 2014 and 2015 (merged) TETFund research project intervention) for this work

Nomenclature

B	Free stream velocity
a, b, c	Constants
C_{fx}	Skin friction coefficient
C	Nanoparticle volume friction
C_w	Nanoparticle volume friction at the sheet surface (wall)
C_∞	Ambient nanoparticle volume friction
D_B	Brownian diffusion coefficient
D_T	Thermophoresis diffusion coefficient
$f'(\eta)$	Dimensionless velocity
h	Convective heat transfer coefficient
k	Thermal conductivity
Le	Lewis number
Nb	Brownian motion parameter
Nt	Thermophoresis parameter
Nu_x	Nusselt number
Pr	Prandtl number
q_w	Wall heat flux
q_r	radiation flux
J_w	Mass flux
Re_x	Local Reynolds number
Sh_x	Sherwood number
T	Fluid temperature
T_f	Hot fluid temperature
T_w	Wall temperature
T_∞	Ambient temperature
u, v	Velocity components
x, y	Coordinates along the sheet
Q	Heat release per unit per time
Ra	Radiation parameter
R_1	Chemical reaction parameter
n	Order of chemical reaction
g	Gravitational force due to gravity
Gr_T	Thermal Grashof number
Gr_C	Solutal Grashof number
B_o	Magnetic field
c_p	Specific heat at constant pressure

Greek Symbol

α_{nf}	Thermal diffusivity
$\varepsilon 1, \delta$	Eyring-Powell fluid constants
θ	Dimensionless temperature
ϕ	Dimensionless nanoparticle volume friction
η	Similarity variable
γ	Biot number (convective surface condition)
μ	Dynamic viscosity of the fluid
υ	Kinematic viscosity
ρ_{nf}	Density

ψ	Stream function
τ_w	Surface shear stress
σ_s	Stefan-Boltzmann constant
σ	Electrical conductivity of the fluid
β_T	Coefficient of thermal expansion
β_C	Coefficient of concentration expansion
λ	Unsteady parameter
λ_1	Internal heat generation

Subscripts

w	Condition at the wall
f	Fluid condition
∞	Ambient condition

Superscript

	Differentiation with respect to η

Conflict of Interest

Authors have declared that there is no conflict of interest related to this study.

References

Alfvén H 1942. Existence of electromagnetic-hydrodynamic waves. *Nature*, 150(3805): 405–406.

Ali F & Zaib A 2019. Unsteady flow of an Eyring-Powell nanofluid near stagnation point past a convectively heated stretching sheet. *Arab J. Basic and Appl. Sci.*, 26(1): 215-224.

Bhatti MM, Abbas T, Rashidi MM, Ali MES & Yang Z 2014. Entropy generation on MHD Erying-Powell nanofluid through a permeable stretching surface. *Entropy*, 18: 1-14.

Buongiorno J 2006. Convective transport in nanofluids. *Journal of Heat Transfer*, 128(3): 240-250.

Chamkha AJ, Aly AM & Mansor MA 2010. Similarity solution for unsteady heat and mass transfer from a stretching surface embedded in a porous medium with suction/injection and chemical reaction effect. *Chemical Engineering Communications*, 197(6): 846-858.

Hajjar Z, Rashidi A & Ghozatloo A 2014. Enhanced thermal conductivities of grapheme oxide nanofluids. *Int. Commun. in Heat and Mass Transfer*, 128-131.

Hayat T, Asad S, Mustafa M & Alsaedi A 2014. Radiation effects on the flow of eyring-powell fluid past an unsteady inclined stretching sheet with uniform heat source/sink. Plos One, 9. Doi.10.1371/journal.pone.0103214.

Heck A 2003. Introduction to Maple. 3rd Edition, Springer-Verlag.

Idowu AS & Falodun BO 2020. Effects of thermophoresis, Soret-Dufouron heat and mass transfer flow of magnetohydrodynamics non-Newtonian nanofluidover an inclined plate. *Arab J. Basic and Appl. Sci.*, 27(1): 149-165, DOI: 10.1080/25765299.2020.1746017

Khan WA & Pop I 2010. Boundary layer flow of a nanofluid past a stretching sheet. *Int. J. Heat Mass Transfer*, 53(11-12): 2477-2483.

Lee S, Kim K & Bang I 2013. Study on flow boiling critical heat flux enhancement of graphene oxide/water nanofluid. *Int. J. Heat and Mass Transfer*, 348-356.

Lin Y, Zheng L, Zhang X, Ma L & Chen G 2015. MHD pseudo-plastic nanofluid unsteady flow and heat transfer in a finite thin film over stretching surface with internal heat generation. *Int. J. Heat Mass Transf*. 84: 903-911.

Madhu M, Kishan N & Chamkha AJ 2017. Unsteady flow of a Maxwell nanofluid over a stretching surface in the presence of magnetohydrodynamic and thermal radiation effects. *Propulsion Power*, 6(1): 31-40.

Mahanthesha B, Gireesha BJ & Gorla RSR 2017. Unsteady three-dimensional eyring-powell fluid past a convectively heated stretching sheet in the presence of thermal radiation, viscous dissipation and joul heating. *J. Assoc. Arab Uni. for Basic and Appl. Sci.*, 23: 75-84.

Makinde OD & Aziz A 2011. Boundary layer flow of nanofluid past stretching sheet with convective boundary condition. *Int. J. Thermal Sci*., 50(7): 1326-1332.

Makinde OD & Olanrewaju PO 2012. Combined effects of internal heat generation and buoyancy force on boundary layer flow over a vertical plate with a convective boundary condition. *Canad. J. Chem. Engr.*, 90: 1289-1294.

Muhammad Khairul Anuar Mohamed, Mohd Zuki Salleh & Anuar Ishak 2020. Effects of viscous dissipation on mixed convection boundary layer flow past a vertical moving plate in a nanofluid. J. Adv. Res. in Fluid Mech. and Thermal Sci., 69(2): 1-18.

Mukhopadhyay S, Ranjan P & De Layek GC 2013. Heat transfer characteristics for the Maxwell fluid flow past an unsteady stretching permeable surface embedded in porous medium with chemical reaction. *J. Appl. Mech. and Technical. Phy.*, 54(3): 385-396.

Olanrewaju PO, Olanrewaju MA & Adesanya AO 2012. Boundary layer flow of nanofluids over a moving surface in a flowing fluid in the presence of radiation. *Int. J. of Appl. Sci. and Techn.*, 2(1): 274-285.

Pop S, Grosan T & Pop I 2004. Radiation effects on the flow near the stagnation point of a stretching sheet. *Tech. Mech*. 25(2): 100-106.

Reddy PBA 2016. MHD boundary layer slip flow of a Casson fluid over an exponentially stretching surface in the presence of thermal radiation and chemical reaction. *J. Naval Arch. Mar. Engr.* 3: 165-177.

Reddy SRR, Reddy P Bala Anki & Rashad AM 2020. Activation energy impact on chemically reacting eyring-powell nanofluid flow over a stretching cylinder. *Arabian J. Sci. and Engr*. https://doi.org/10.1007/s13369-020-04379-9.

Sharma A, Tiwari A & Dixit A 2016. Rheological behaviour of nanofluids: A review. *Renewable and Sustainable Energy Reviews*, 779-791.

Shateyi S, Motsa SS & Sibanda P 2010. The effects of thermal radiation, hall currents, Soret, and Dufour on MHD flow by mixed convection over a vertical surface in porous media. *Mathematical Problems in Engineering*, Article ID 627475, 20 pages. Doi: 10.1155/2010/627475.

Sharifpur M, Adio S & Meyer J 2015. Experimental investigation and model developmentfor effective viscosity of Al2O3–glycerol nanofluids by using dimensional analysis and GMDH-NN methods. *Int. Commun. in Heat and Mass Transfer*, 208-219.

Srinivas S, Reddy PBA & Prasad BSRV 2014. Effects of chemical reaction and thermal radiation on MHD flow over an inclined permeable stretching surfaces with non-uniform heat source/sink: an application to the dynamics of blood flow. *J. Mech. Med. Biol*., 14(05): 1450067.